Ultrasound Elasticity Imaging for Determining the Mechanical Properties of Human Posterior Tibial Tendon: A Cadaveric Study

Liang Gao*, Justin S. Yuan, Gregory J. Heden, John A. Szivek, Mihra S. Taljanovic, L. Daniel Latt, and Russell S. Witte

***Abstract*—Posterior tibial tendon dysfunction (PTTD) is a common degenerative condition leading to a severe impairment of gait. There is currently no effective method to determine whether a patient with advanced PTTD would benefit from several months of bracing and physical therapy or ultimately require surgery. Tendon degeneration is closely associated with irreversible degradation of its collagen structure, leading to changes to its mechanical properties. If these properties could be monitored *in vivo*, they could be used to quantify the severity of tendonosis and help determine the appropriate treatment. The goal of this cadaveric study was, therefore, to develop and validate ultrasound elasticity imaging (UEI) as a potentially noninvasive technique for quantifying tendon mechanical properties. Five human cadaver feet were mounted in a materials testing system (MTS), while the posterior tibial tendon (PTT) was attached to a force actuator. A portable ultrasound scanner collected 2-D data during loading cycles. Young's modulus was calculated from the strain, loading force, and cross-sectional area of the PTT. Average Young's modulus for the five tendons was (0.45 ± 0.16 GPa) using UEI, which was consistent with simultaneous measurements made by the MTS across the whole tendon (0.52 ± 0.18 GPa). We also calculated the scaling factor (0.12 ± 0.01) between the load on the PTT and the inversion force at the forefoot, a measurable quantity *in vivo*. This study suggests that UEI could be a reliable *in vivo* technique for estimating the mechanical properties of the PTT, and as a clinical tool, help guide treatment decisions for advanced PTTD and other tendinopathies.**

***Index Terms*—Posterior tibial tendon dysfunction (PTTD), strain imaging, tendinopathy, ultrasound elastography, Young's modulus.**

I. Introduction

THE primary function of the posterior tibial tendon (PTT) is to invert the foot and restore the arch during the stance phase of gait. It is highly susceptible to overuse injury and degeneration, leading to an acquired flatfoot deformity and difficulty with ambulation. Posterior tibial tendon dysfunction (PTTD) is especially common in women over 40 years of age with an incidence of 3.3% [1].

The pathophysiology of PTTD involves localized tendon degeneration behind the medial malleolus, where the tendon experiences maximal stress and poor blood supply [2]. It is thought that irreversible degradation of collagen structure leads to lengthening of the tendon, change in mechanical properties [3], and eventually a collapse of the medial longitudinal arch. Several studies have confirmed the link between tendinopathy and changes in the elastic properties of tendon [4]–[6]. One study of Achilles tendinopathy reported a 51% decrease in Young's modulus (1.67–0.82 GPa) of the Achilles tendon as compared to healthy controls [7]. Another found that strength training for the Achilles in the elderly led to a 69% increase in Young's modulus (1.3–2.2 GPa) [8].

Stage II PTTD (flexible flatfoot deformity) is often treated with surgery using tendon transfer to restore inversion power and osteotomies (reshaping of the bones) to reconstruct the arch and restore proper alignment of the heel. However, recent studies suggest that 60–90% of these patients respond to nonoperative treatment consisting of bracing and physical therapy for 3–6 months [9]–[14]. Moreover, many of these patients (33–70%) were able to resume normal gait and become brace free. However, there is no reliable method to predict which patients will do well with conservative care and which will ultimately require surgery [15]. This has led to prolonged unsuccessful conservative treatment in some patients and premature surgical intervention in others. Thus, there is a great need for an objective evidence-based tool to evaluate the PTT, help classify advanced-stage PTTD, determine its prognosis, and inform treatment decisions. Unfortunately, a noninvasive clinical tool for quantifying a tendon's mechanical properties does not currently exist.

To overcome this limitation, we propose ultrasound elasticity imaging (UEI) as a noninvasive technique for quantifying the stiffness and elastic properties of the PTT. UEI consists of acquiring a sequence of ultrasound frames and applying speckle tracking to estimate displacement and strain at each pixel [16]–[24]. The technique is FDA approved for diagnostic breast imaging and classifying suspicious lesions based on the strain pattern, leading to a reduction of unnecessary biopsies [25]. Other clinical applications include assessing contractility

Manuscript received September 6, 2014; revised November 14, 2014; accepted December 1, 2014. Date of publication December 18, 2014; date of current version March 17, 2015. This work was supported in parts by the BIO5 Institute, Orthopedic Research & Education Foundation, and Technology and Research Initiative Fund. *Asterisks indicate corresponding authors.*

*L. Gao is with the College of Optical Sciences, University of Arizona, Tucson, AZ 85721 USA (e-mail: lgao@email.arizona.edu).

J. S. Yuan and G. J. Heden are with the College of Medicine, University of Arizona.

J. A. Szivek and L. D. Latt are with the Department of Orthopaedic Surgery, University of Arizona.

M. S. Taljanovic is with Department of Medical Imaging, University of Arizona.

R. S. Witte is with Biomedical Engineering, Optical Sciences, University of Arizona.

Color versions of one or more of the figures in this paper are available online at http://ieeexplore.ieee.org.

Digital Object Identifier 10.1109/TBME.2014.2381002

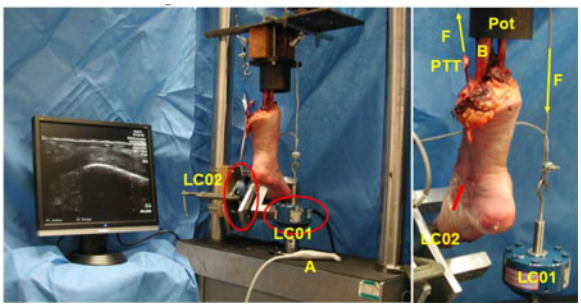

Fig. 1. (Left) Photograph of the experimental setup, including the MTS and the 14-MHz hockey stick linear array ("A"). The monitor displays a B-mode image of the PTT. The primary load cell ("LC01") measured the load force ("F") applied to the tendon, while a secondary load cell ("LC02") measured the inversion force. (Right) Closer view from a reverse angle displaying imaging side of the foot. The primary load cell ("LC01") pulled the PTT proximally via a steel cable. The yellow arrows denote the direction of pulling while loading. The foot was potted in a Cerrobend pot ("Pot") using the fibula and tibia ("B"). The red line near the ankle marks the standard position of the ultrasound probe over the PTT.

and strain deficiencies in the myocardium and quantifying mechanical properties of tissue-engineered implants [26]–[31]. Several recent studies have implemented UEI to quantify the mechanical properties of human skeletal muscle and tendon (electrically stimulated or under load) [4], [32]–[40]. However, none of these studies employed elasticity imaging to quantify differences in tendon mechanical properties associated with degeneration or rehabilitation.

The primary goal of this project was to develop and validate the UEI technique of the human PTT using a cadaver model and to obtain baseline estimates of its mechanical properties. A secondary goal was to determine the relationship between the tensile force applied to the PTT and the corresponding inversion force generated at the forefoot, which is a measurable parameter for future *in vivo* experiments. The long-term goal was to create a quantitative *in vivo* test that can be employed clinically for grading degenerative tendon diseases, aiding in prognosis, and helping guide treatment decisions.

II. Methods

Five thawed human cadaver feet from male and female donors aged from 68 to 92 years were transected midleg, potted in a Cerrobend pot, and mounted in a materials testing system (MTS, Model 810 Systems Corporation, Eden Prairie, MN). The proximal portion of the PTT was dissected free from the muscle, whipstitched with high strength suture, and attached via a steel cable to a load cell mounted on an actuator (see Fig. 1). The exposed portion was wrapped with gauze soaked in saline to prevent desiccation.

A commercial 14-MHz linear array ultrasound probe (L14–5, Zonare Medical Systems, Mountain View, CA, USA) was positioned over the PTT adjacent to the medial malleolus. This portion of the tendon was chosen because it is most vulnerable to degeneration and most often affected by PTTD. The probe was connected to a portable ultrasound scanner (zOneUltra, Zonare Medical Systems) controlled by a PC running MATLAB (Mathworks Inc.) to acquire ultrasound frame data (both amplitude and phase) at a rate of 50 Hz for 6 s. The ultrasound

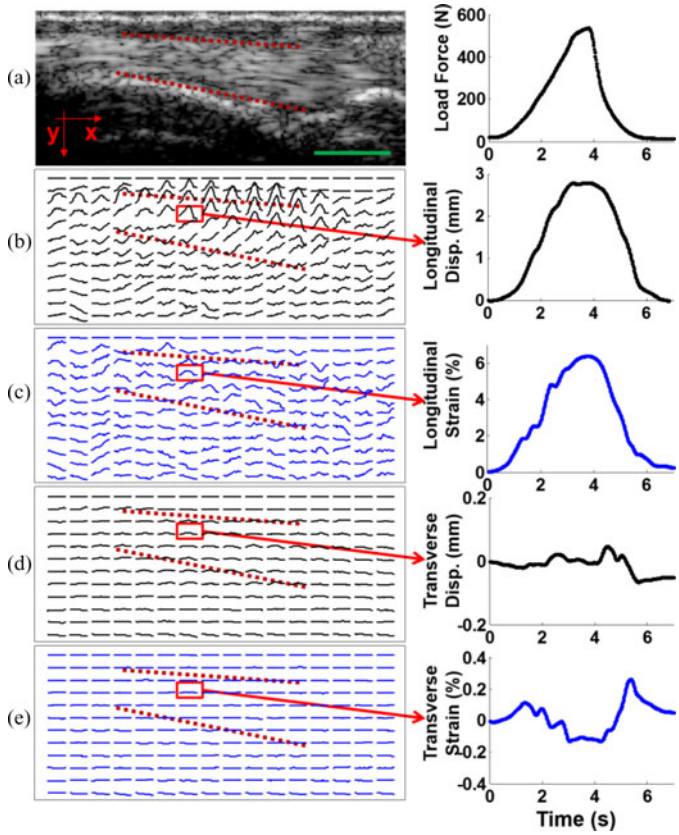

Fig. 2. UEI displacement and strain of the PTT during a representative loading–unloading cycle. (Left column, from top) B-mode image with PTT between two red dotted lines, longitudinal (x) displacement, longitudinal strain, transverse (y) displacement, and transverse strain over small regions (1.5×0.5 mm). The green scale bar in the image $=$ 5 mm. (Right column, from top) Force measured at the proximal end of the PTT by the primary load cell, longitudinal displacement (Disp.), longitudinal strain, transverse displacement, and transverse strain in the region enclosed by the red box in the left column.

probe was held by an experienced sonographer with its long axis aligned parallel to the PTT.

A preload of 10 N was applied to maintain the tendon under tension. The specimen was then subjected to three load–unload cycles. Each cycle lasted for 5 s, during which the axial force was gradually increased from preload to 588 N (60 kg, approximating the weight of an adult female), and the tendon was then allowed to return to preload. Inversion force measurements were obtained during the trial from a second load cell that abutted the medial aspect of the first metatarsal head. Stroke of the actuator, representing the displacement of the proximal end of the PTT, was recorded by the MTS machine.

Transverse B-mode images were used to determine the cross-sectional area (CSA), denoted as A, of each PTT. The boundary of the tendon was traced three times at three different locations (inframalleolar, retromalleolar, and supramalleolar), and the average area was used to calculate tendon stress. The total length of the PTT was measured at the conclusion of the experiment.

Frame-to-frame displacements were calculated during the loading portion of each cycle. A 2-D phase sensitive cross correlation algorithm, described previously for other biomedical

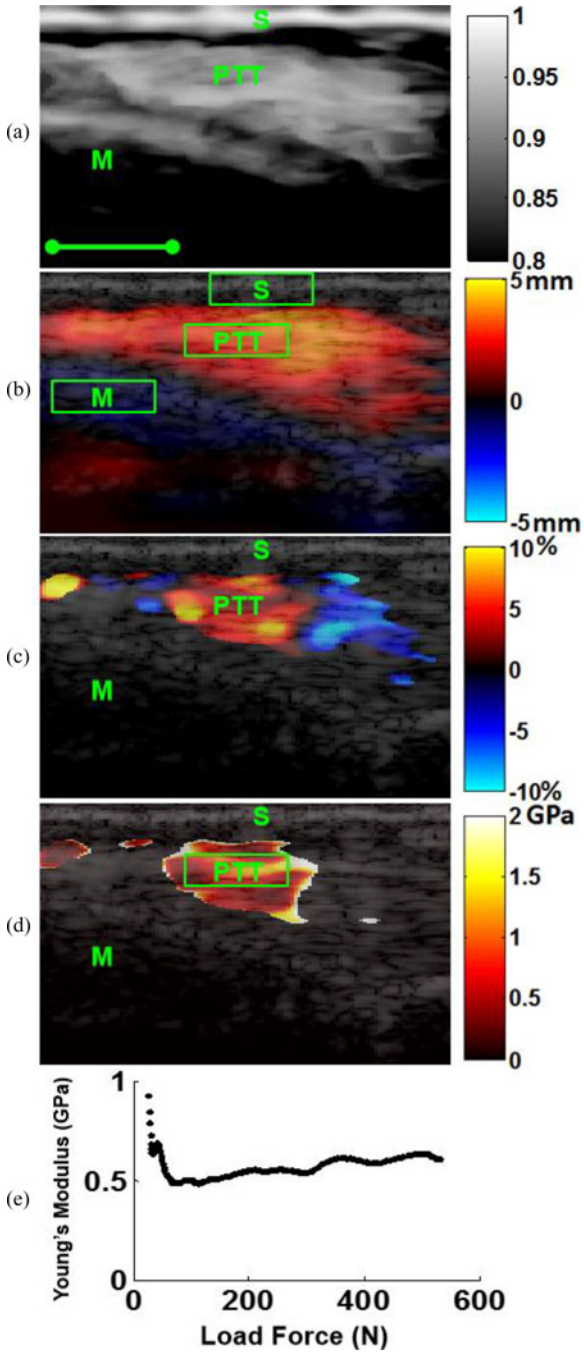

Fig. 3. (a) 2-D Map of the speckle tracking correlation coefficient (average over one cycle). Green scale bar = 5 mm, S = Skin, M = Malleolus. (b) Longitudinal displacement map. The three boxes denote the ROIs used to calculate the displacement within and outside the tendon. (c) Strain map at a near maximal load (550 N) superimposed on the B-mode image (gray). (d) Image of Young's modulus in tendon above malleolus. The discontinuity in the strain map was due to out-of-plane motion of the PTT as it turned around the ankle joint. This was more evident in the B-mode movies. (e) Young's modulus versus loading force, averaged over the green box in (d).

applications [23], [24], [34], [41], produced a displacement map along both directions at each pixel location in the ultrasound image, along with the correlation map ("trashogram") for estimating tracking confidence. Strain was calculated from the displacement along the tendon axis (longitudinal, or x direction): For each pixel, the longitudinal stain S_{xx} was calculated from $S_{xx} = (d_2 - d_1)/L$, where d_1 and d_2 are the displacements at each end of the window of length L. This was repeated across the entire image, yielding longitudinal strain information throughout the tendon and surrounding structures within the B-mode image. Finally, the loading force (F) recorded by the MTS was used to calculate stress σ from $\sigma = F/A$. Young's modulus E_{xx} was then computed by dividing the estimated stress by the measured strain ($E_{xx} = \sigma/S_{xx}$).

To isolate the tendon from background structures, and automatically choose a region of interest (ROI), principle component analysis (PCA) was performed on the lateral displacement maps during the load cycle. Because the PTT has larger displacements and velocities compared to the surrounding tissue, the peak of the first principal component was always within the PTT. The ROI was then chosen to be a rectangular region ($3.9\ \mathrm{mm} \times 1.2\ \mathrm{mm}$) centered at the weighted centroid of the first principal component for each trial. The mean and standard deviation (SD) of the displacement, strain, and Young's modulus of the PTT were calculated over this ROI across multiple trials.

For this cadaveric study, UEI measurements were compared with the MTS as the gold standard for estimating Young's modulus for the entire tendon. The stroke (displacement) recorded by the MTS was expected to be larger than the displacement from UEI, because the former represents the displacement of the tendon at the free end and the latter the displacement at a region near the fixed end. Nevertheless, the two should be strongly correlated. Stroke was converted to strain for the MTS using the total length of the PTT. For comparison and validation of UEI with MTS, we expected the strain values to be similar for the two techniques. Furthermore, the average Young's modulus determined by the MTS over the entire tendon was calculated using the same equations described previously and compared with that of UEI. The coefficient of determination (R^2) between UEI and MTS was also calculated across the specimens for displacement, strain, and Young's modulus.

Finally, to further verify the accuracy of UEI, we compared video tracking of surface strain with ultrasound strain estimates in one tendon. This validation was performed in the supramalleolar portion of the PTT, as it was not practical to perform video tracking in the retromalleolar position where the tendon bends around the malleolus. UEI was first performed with the skin intact and the imaging location marked. The skin at the marked location, subcutaneous tissue, and tendon sheath were then dissected to expose the surface of the PTT. Fiducial ink marks were placed on the tendon surface. The same load–unload cycle was performed, and the movement of the PTT was recorded using a digital camera (Canon G12). Video strain was estimated using a motion analysis software package (Tracker, Video Analysis, and Modeling Tool [42]). The coefficient of determination (R^2) and mean difference were then calculated to compare UEI and video tracking strain values.

III. Results

UEI displacement and strain maps for a representative PTT are displayed in Fig. 2. The primary motion and deformation occurred along the longitudinal axis of the tendon.

TABLE I
SUMMARY OF TENDON SIZES AND MECHANICAL PROPERTIES

Specimen	CSA [mm^2]	Length [mm]	Displacement [mm]		Strain [%]		Young's Modulus [GPa]	
			MTS	UEI	MTS	UEI	MTS	UEI
1	23.0 ± 3.8	210	6.5 ± 0.8	1.3 ± 0.8	3.1 ± 0.2	3.7 ± 0.8	0.78 ± 0.05	0.66 ± 0.14
2	24.8 ± 0.6	215	11.1 ± 0.4	3.3 ± 0.1	5.2 ± 0.2	5.3 ± 0.3	0.43 ± 0.02	0.42 ± 0.03
3	30.8 ± 1.5	230	13.0 ± 0.3	3.6 ± 1.3	5.7 ± 0.1	7.2 ± 1.9	0.32 ± 0.01	0.26 ± 0.04
4	31.3 ± 1.8	180	7.5 ± 0.1	1.6 ± 0.6	4.2 ± 0.1	5.0 ± 0.5	0.43 ± 0.01	0.36 ± 0.04
5	28.1 ± 1.6	210	6.6 ± 0.4	1.9 ± 0.7	3.2 ± 0.2	3.6 ± 0.9	0.62 ± 0.04	0.57 ± 0.15
Mean $\pm$ SD	27.6 ± 3.6	209 ± 18	8.9 ± 2.9	2.3 ± 1.0	4.2 ± 1.2	5.0 ± 1.5	0.52 ± 0.18	0.45 ± 0.16

The longitudinal displacement, strain, and Young's modulus values were at near-maximal force (550 N). The donor ages for the five specimens ranged from 68 to 92 years old. Specimen 3 and 5 were from male donors.

Fig. 3 presents a map of the 2-D speckle tracking correlation coefficient, longitudinal displacement, strain, and Young's modulus for one tendon at an applied load of 550 N. The displacement map [see Fig. 3(b)] clearly identifies the tendon from surrounding tissue. The displacement within the tendon (3.33 ± 0.23 mm) over the ROI displayed in Fig. 3(b), is much higher than the displacement outside the tendon (0.87 ± 0.04 and 0.09 ± 0.08 mm in the malleolus and the dermal layers, respectively).

Table 1 lists the tendon CSA, total tendon length, longitudinal displacement, strain, and Young's modulus of each specimen.

Fig. 4 compares results for the MTS and UEI for measuring displacement ($R^2 = 0.95$), strain ($R^2 = 0.88$), and Young's modulus ($R^2 = 0.96$). The average Young's modulus for the five tendons calculated from UEI was 0.45 ± 0.16 GPa, compared with 0.52 ± 0.18 GPa for measurements from the MTS.

Fig. 5 directly compares strain measurements obtained using UEI with those using video tracking for one tendon. Video strain at the surface of the tendon was similar to UEI measurements within the tendon ($R^2 = 0.80$). The mean difference between the two strain curves was $0.11 \pm 0.03\%$.

Fig. 6 describes the relationship between the applied load and inversion force recorded by the load cell. The slope and R^2 values were 0.12 ± 0.01 and 0.999, respectively, indicating that the inversion force is approximately one eighth of the applied load. The relationship between the inversion force, a measurable quantity *in vivo*, and the force on the tendon is an important parameter for potential clinical applications of UEI in PTTD patients.

IV. DISCUSSION

The primary goal of this study was to develop and validate the technique of UEI of the PTT. Our results indicate that UEI is capable of accurately measuring the mechanical properties of the human PTT in a cadaveric model. UEI estimates of displacement, strain, and Young's modulus were all highly correlated with those obtained from the stroke of the MTS crosshead (see Fig. 4). There was a close agreement between Young's modulus for UEI (0.45 ± 0.16 GPa) and MTS (0.52 ± 0.18 GPa). Differences could be explained by regional variations in the measurements. Whereas UEI measured the mechanical properties over a small, high-stress region above the malleolus, the

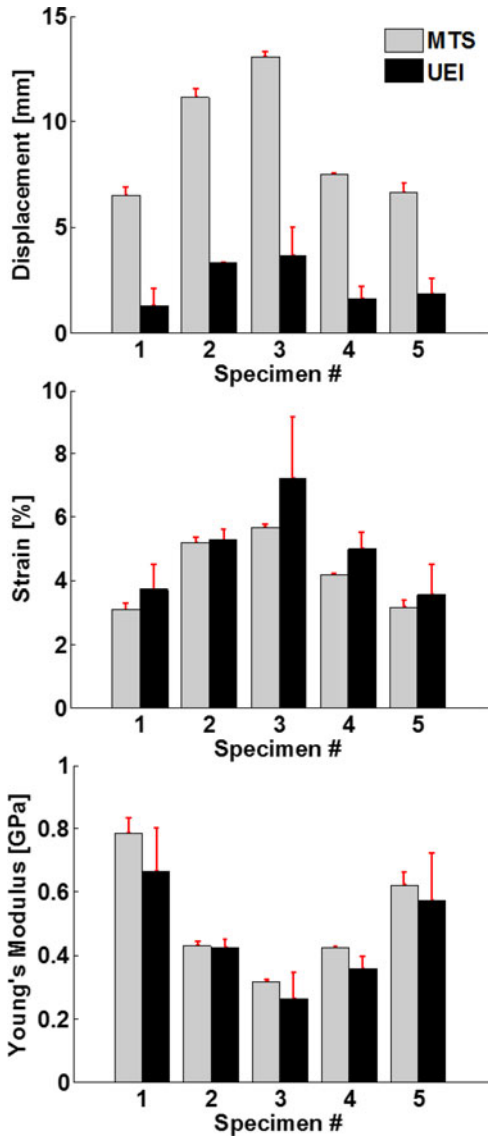

Fig. 4. Comparison of longitudinal displacement (Top), strain (Middle), and Young's modulus (Bottom) using MTS (gray, entire tendon) and UEI (black, localized region). All values were calculated at 550 N. The red error bar denotes standard deviation (SD), which was calculated for each specimen over three trials. The displacement for the MTS was much larger than UEI because the MTS measurement occurred across the entire tendon rather than just the local region above the malleolus. Nevertheless, there was a high correlation between UEI and MTS for displacement ($R^2 = 0.95$), strain ($R^2 = 0.88$), and Young's modulus ($R^2 = 0.96$) for the five specimens.

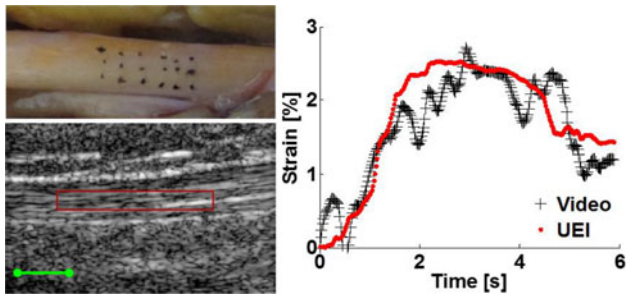

Fig. 5. Comparison between video tracking and UEI for measuring strain for the same tendon at supramalleolar location. (Top Left) Photograph of top surface of tendon with fudicial ink markers placed for optical tracking. (Bottom Left) Ultrasound image at the same location, green bar = 5 mm. (Right). Strain measured at the surface of the PTT using video (black) and within the PTT using UEI (red). The average strain for UEI was computed over the red box in the B-mode image. The mean difference between the two strain curves was $0.11 \pm 0.03\%$.

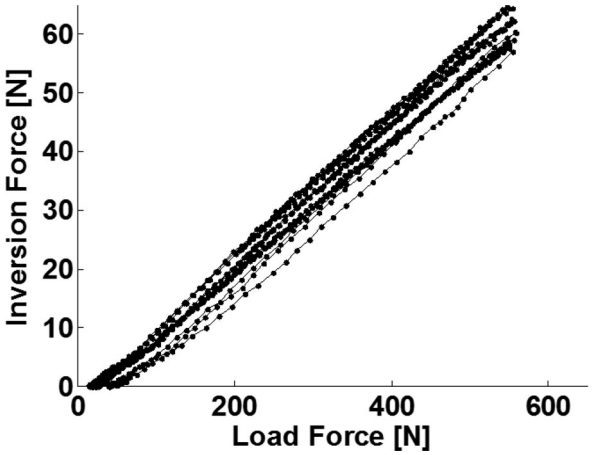

Fig. 6. Relationship between applied load and inversion force for five PTTs. This plot includes results for three trials for each of the samples. The average slope is 0.12 ± 0.01 with $R^2 = 0.999$.

MTS recorded an average value across the entire length of the tendon. The tendon might also be more compliant in the imaged retromalleolar region. Moreover, dynamic video tracking of surface strain was highly consistent with ultrasound strain estimates (see Fig. 5).

Two previous studies measured Young's modulus of the dissected PTT (0.81 ± 0.14 GPa and 0.91 ± 0.23 GPa) [43], [44]. However, these values were at a much higher tendon load (2500 and 3600 N) than our study (588 N). Based on the load–displacement curve provided in one of these studies, Young's modulus was approximately 0.45 GPa at 600 N [44], which is similar to our result.

One potential limitation with this project relates to the use of thawed cadaveric specimens. There is evidence that freezing followed by thawing alters the structure and mechanical properties of the tendon [43]. That study found that frozen specimens of the human posterior tibial tendon, compared to fresh specimens, exhibited 30% lower stress and strain than fresh specimens primarily due to a decrease in collagen fibril density. However, Young's modulus was not significantly different between the two groups, implying that Young's modulus for thawed PTTs is likely similar to fresh PTTs.

Another potential limitation of the study relates to speckle tracking noise and out-of-plane motion of the tendon. For optimal imaging, it is important that the sonographer maintain the probe parallel to the long axis of the PTT during the loading phase. The speckle tracking coefficient and B-mode movie provide feedback for the quality of the images. Fig. 3(c) provides evidence of out-of-plane motion of a portion of the tendon as it turned around the malleolus bone. This led to a nonuniform strain pattern. In addition, because the primary motion of the tendon was along its axis, transverse displacements and strain were much smaller compared to longitudinal displacements. The transverse displacement and strain would likely be more sensitive to deformation at the tissue interfaces and pressure applied by the ultrasound probe, while less sensitive to the transverse deformation of the PTT. Nonetheless, the transverse displacements were not used for calculating the mechanical properties of the tendon.

UEI is a potentially powerful, noninvasive *in vivo* technique to objectively quantify the mechanical proprieties of the PTT and other tendons. This would require estimating tensile load (or stress) noninvasively, which is a challenge *in vivo*. In this study, the load applied to the PTT and the resulting inversion force at the forefoot were simultaneously measured. Their relationship was linear with a slope between the inversion force and tendon load of 0.12 ± 0.01. This value could be used to estimate tensile load from the measured inversion force obtained *in vivo*. A similar approach was successfully implemented in a study of the human Achilles tendon [45]. For *in vivo* human testing, it would be necessary to fix the ankle in maximal plantar flexion so that other tendons would not be able to contribute to inversion of the foot. It would also be necessary to brace the lateral malleolus to prevent lateral translation of the ankle. The development of techniques for precise and accurate measurement of the inversion force would be an important step in the development of UEI as a clinical tool for guiding treatment of tendinopathies.

In conclusion, we have demonstrated that ultrasound elastography reliably quantifies the mechanical properties of the PTT in a human cadaveric model. This is an important first step in the development of UEI as a clinical tool for objectively quantifying tendon mechanical properties in patients with tendinopathies. Such a clinical tool could aid in the prognosis, guide treatment decision making, and monitor response to treatment for a number of degenerative tendon disorders, including PTTD.

REFERENCES

[1] J. Kohls-Gatzoulis *et al.*, "The prevalence of symptomatic posterior tibialis tendon dysfunction in women over the age of 40 in England," *Foot Ankle Surg.*, vol. 15, no. 2, pp. 75–81, 2009.

[2] W. Petersen *et al.*, "The blood supply of the posterior tibial tendon," *J. Bone Joint Surg. Brit.*, vol. 84, no. 1, pp. 141–4, 2002.

[3] G. C. Pomeroy *et al.*, "Acquired flatfoot in adults due to dysfunction of the posterior tibial tendon," *J. Bone Joint Surg. Amer.* vol. 81, no. 8, pp. 1173–82, 1999.

[4] C. N. Maganaris and J. P. Paul, "In vivo human tendon mechanical properties," *J. Physiol.* vol. 521, pp. 307–313, 1999.

[5] G. A. Lichtwark and A. M. Wilson, "In vivo mechanical properties of the human Achilles tendon during one-legged hopping," *J. Exp. Biol.*, vol. 208, pp. 4715–25, 2005.
[6] H. Zhao *et al.*, "Ultrasonic evaluations of Achilles tendon mechanical properties post stroke," *J. Appl. Physiol.*, vol. 106, pp. 843–849, 2009.
[7] S. Arya and K. Kulig, "Tendinopathy alters mechanical and material properties of the Achilles tendon," *J. Appl. Physiol.*, vol. 108, pp. 670–675, 2010.
[8] N. D. Reeves *et al.*, "Effect of strength training on human patella tendon mechanical properties of older individuals," *J. Physiol.*, vol. 548, pp. 971–981, 2003.
[9] J. F. Augustin, "Nonoperative treatment of adult acquired flat foot with the Arizona brace," *Foot Ankle Clinics*, vol. 8, no. 3, pp. 491–502, 2003.
[10] R. G. Alvarez, "Stage I and II posterior tibial tendon dysfunction treated by a structured nonoperative management protocol: An orthosis and exercise program," *Foot Ankle Int.* vol. 27, no. 1, pp. 2–8, 2006.
[11] J. L. Lin *et al.*, "Results of non-surgical treatment of stage II posterior tibial tendon dysfunction: A 7 to 10-year followup," *Foot Ankle Int.*, vol. 29, no. 8, pp. 781–6, 2008.
[12] M. D. Nielsen, "Nonoperative care for the treatment of adult-acquired flatfoot deformity," *J. Foot Ankle Surg.*, vol. 50, no. 3, pp. 311–4, 2011.
[13] K. Kulig, "Nonsurgical management of PTTD with orthoses and resistive exercise: A randomized controlled trial," *Phys. Therapy*, vol. 89, no. 1, pp. 26–37, 2009.
[14] W. Chao, *et al.*, "Nonoperative management of posterior tibial tendon dysfunction," *Foot Ankle Int.*, vol. 17, no. 12, pp. 736–741, 1996.
[15] K. A. Johnson and D. E. Strom, "Tibialis posterior tendon dysfunction," *Clin. Orthopaedics Related Res.*, vol. 239, pp. 196–206, 1989.
[16] J. Ophir *et al.*, "Elastography: A quantitative method for imaging the elasticity of biological tissues," *Ultrason Imaging*, vol. 13, pp. 111–134, 1991.
[17] A. R. Skovoroda *et al.*, "Theoretical analysis and verification of ultrasound displacement and strain imaging," *IEEE Trans. Ultrason. Ferroelectr. Freq. Control*, vol. 41, no. 3, pp. 302–313, May 1994.
[18] M. O'Donnell *et al.*, "Internal displacement and strain imaging using ultrasonic speckle tracking," *IEEE Trans. Ultrason. Ferroelectr. Freq. Control*, vol. 41, no. 3, pp. 314–325, May 1994.
[19] M. Bilgen and M. F. Insana, "Deformation models and correlation analysis in elastography," *J. Acoust. Soc. Amer.*, vol. 99, pp. 3212–3224, 1996.
[20] M. A. Lubinski *et al.*, "Speckle tracking methods for ultrasonic elasticity imaging using short-time correlation," *IEEE Trans. Ultrason. Ferroelectr. Freq. Control*, vol. 46, no. 1, pp. 82–96, Jan. 1999.
[21] K. Kaluzynski *et al.*, "Strain rate imaging using two-dimensional speckle tracking," *IEEE Trans. Ultrason. Ferroelectr. Freq. Control*, vol. 48, no. 4, pp. 1111–1123, Jul. 2001.
[22] M. Leitman *et al.*, "Two-dimensional strain—A novel software for real-time quantitative echocardiographic assessment of myocardial function," *J. Amer. Soc. Echocardiography*, vol. 17, pp. 1021–1029, 2004.
[23] Y. Notomi *et al.*, "Measurement of ventricular torsion by two-dimensional ultrasound speckle tracking," *J. Amer. College Cardiol.*, vol. 45, pp. 2034–2041, 2005.
[24] W.-N. Lee *et al.*, "Theoretical quality assessment of myocardial elastography with in vivo validation," *IEEE Trans. Ultrason. Ferroelectr. Freq. Control*, vol. 54, no. 11, pp. 2233–2245, Nov. 2007.
[25] M. Roach 3rd, *et al.*, "Diagnostic and therapeutic imaging for cancer: Therapeutic considerations and future directions," *J. Surg. Oncol.*, vol. 103, no. 6, pp. 587–601, 2011.
[26] J. D'hooge *et al.*, "Two-dimensional ultrasonic strain rate measurement of the human heart in vivo," *IEEE Trans. Ultrason. Ferroelectr. Freq. Control*, vol. 49, no. 2, pp. 281–286, Feb. 2002.
[27] J. D'hooge *et al.*, "Echocardiographic strain and strain-rate imaging: A new tool to study regional myocardial function," *IEEE Trans. Med. Imaging*, vol. 21, no. 9, pp. 1022–1030, Sep. 2002.
[28] M. Uematsu *et al.*, "Myocardial velocity gradient as a new indicator of regional left ventricular contraction: Detection by a two-dimensional tissue Doppler imaging technique," *J. Amer. College Cardiol.*, vol. 26, pp. 217–223, 1995.
[29] S. Urheim *et al.*, "Myocardial strain by Doppler echocardiography. Validation of a new method to quantify regional myocardial function," *Circulation*, vol. 102, no. 10, pp. 1158–1164, 2000.
[30] C. Jia *et al.*, "Two-dimensional strain imaging of controlled rabbit hearts," *Ultrasound Med. Biol.*, vol. 35, no. 9, pp. 1488–501, Sep. 2009.
[31] K. Kim *et al.*, "Non-invasive monitoring of tissue scaffold degradation using ultrasound elasticity imaging," *Acta Biomaterialia*, vol. 4, no. 4, pp. 783–90, 2008.
[32] R. S. Witte *et al.*, "High resolution ultrasound imaging of skeletal muscle dynamics and effects of fatigue," in: *Proc. IEEE Ultrason. Symp.*, 2004, pp. 764–767.
[33] R. S. Witte *et al.*, "Effect of fatigue on muscle elasticity in the human forearm using ultrasound strain imaging," in *Proc. 28th IEEE Eng. Med. Biol. Soc.*, 2006, pp. 4490–4493.
[34] R. S. Witte *et al.*, "Least-squares spline for reducing tracking error in muscle strain imaging," in *Proc. 6th Int. Tissue Elasticity Conf.* 2007, p. 97.
[35] J. Farron *et al.*, "Measurement of tendon strain during muscle twitch contractions using ultrasound elastography," *IEEE Trans. Ultrason. Ferroelectr. Freq. Control*, vol. 56, no. 1, pp. 27–35, Jan. 2009.
[36] L. A. Chernak and D. G. Thelen, "Tendon motion and strain patterns evaluated with two-dimensional ultrasound elastography," *J. Biomech.*, vol. 45, no. 15, pp. 2618–2623, 2012.
[37] P. G. Brown *et al.*, "The AutoQual ultrasound elastography method for quantitative assessment of lateral strain in post-rupture Achilles tendons," *J. Biomech.*, vol. 46, no. 15, pp. 2695–2700, Oct. 2013.
[38] E. E. Drakonaki *et al.*, "Real-time ultrasound elastography of the normal Achilles tendon: Reproducibility and pattern description," *Clin. Radiol.*, vol. 64, no. 12, pp. 1196–1202, 2009.
[39] Y. Yoshii *et al.*, "Ultrasound assessment of the motion patterns of human flexor digitorum superficialis and profundus tendons with speckle tracking," *J. Orthopaedic Res.*, vol. 29, no. 10, pp. 1465–1469, 2011.
[40] Y. S. Kim *et al.*, "In vivo strain analysis of the intact supraspinatus tendon by ultrasound speckles tracking imaging," *J. Orthopaedic Res.*, vol. 29, no. 12, pp. 1931–1937, 2011.
[41] S. W. Huang *et al.*, "Analysis of correlation coefficient filtering in elasticity imaging," *IEEE Trans. Ultrason. Ferroelectr. Freq. Control*, vol. 55, no. 11, pp. 2426–2441, Nov. 2008.
[42] (2014). [Online]. Available: https://www.cabrillo.edu/∼dbrown/tracker/
[43] S. Giannini *et al.*, "Effects of freezing on the biomechanical and structural properties of human posterior tibial tendons," *Int. Orthopaedics*, vol. 32, no. 2, pp. 145–151, 2008.
[44] T. L. Haut Donahue *et al.*, "A biomechanical evaluation of anterior and posterior tibialis tendons as suitable single-loop anterior cruciate ligament grafts," *Arthroscopy*, vol. 18, no. 6, pp. 589–97, 2002.
[45] N. D. Reeves *et al.*, "Influence of 90-day simulated microgravity on human tendon mechanical properties and the effect of resistive countermeasures," *J. Appl. Physiol.*, vol. 98, no. 6, pp. 2278–2286, 2005.

Authors' photographs and biographies not available at the time of publication.